





High-Energy Heavy Ion Tracks in Nanocrystalline Silicon Nitride

Arno Janse van Vuuren ^{1,*}, Alisher Mutali ^{2,3,4}, Anel Ibrayeva ^{1,3,4}, Alexander Sohatsky ², Vladimir Skuratov ^{2,5,6}, Abdirash Akilbekov ⁴, Alma Dauletbekova ⁴ and Maxim Zdorovets ^{3,4,7}

¹ Centre for HRTEM, Nelson Mandela University, Port Elizabeth 6001, South Africa

² Flerov Laboratory of Nuclear Research, Joint Institute for Nuclear Research, 141980 Dubna, Russia

³ Institute of Nuclear Physics, Almaty 050032, Kazakhstan

⁴ Physics & Techniques, L.N. Gumilyov Eurasian National University, Nur-Sultan 010000, Kazakhstan

⁵ Institute of Nuclear Physics and Engineering, National Research Nuclear University MEPhI, 115409 Moscow, Russia

⁶ Department of Nuclear Physics, Dubna State University, 141982 Dubna, Russia

⁷ Department of Physics, Ural Federal University, 620075 Yekaterinburg, Russia

* Correspondence: arnojv@gmail.com

Abstract: At present, silicon nitride is the only nitride ceramic in which latent ion tracks resulting from swift heavy ion irradiation have been observed. Data related to the effects of SHIs on the nanocrystalline form of Si₃N₄ are sparse. The size of grains is known to play a role in the formation of latent ion tracks and other defects that result from SHI irradiation. In this investigation, the effects of irradiation with high-energy heavy ions on nanocrystalline silicon nitride is studied, using transmission electron microscopy techniques. The results suggest that threshold electronic stopping power, S_{et} , lies within the range 12.3 ± 0.8 keV/nm to 15.2 ± 1.0 keV/nm, based on measurements of track radii. We compared the results to findings for polycrystalline Si₃N₄ irradiated under similar conditions. Our findings suggest that the radiation stability of silicon nitride is independent of grain size.

Keywords: Si₃N₄ silicon nitride; swift heavy ions; latent ion tracks; transmission electron microscopy (TEM)



Citation: Janse van Vuuren, A.; Mutali, A.; Ibrayeva, A.; Sohatsky, A.; Skuratov, V.; Akilbekov, A.; Dauletbekova, A.; Zdorovets, M. High-Energy Heavy Ion Tracks in Nanocrystalline Silicon Nitride. *Crystals* **2022**, *12*, 1410. <https://doi.org/10.3390/cryst12101410>

Academic Editors: Anton Meden and Tadej Rojac

Received: 14 September 2022

Accepted: 2 October 2022

Published: 5 October 2022

Publisher's Note: MDPI stays neutral with regard to jurisdictional claims in published maps and institutional affiliations.



Copyright: © 2022 by the authors. Licensee MDPI, Basel, Switzerland. This article is an open access article distributed under the terms and conditions of the Creative Commons Attribution (CC BY) license (<https://creativecommons.org/licenses/by/4.0/>).

1. Introduction

Nuclear waste storage is one of the main obstacles to the adoption of nuclear energy as a sustainable source. The most optimal situation would be to have a fuel cycle that is either partly or fully closed. To facilitate this optimal situation, nuclear waste would need to be reprocessed or reintegrated into the fuel cycle. One means of achieving this goal is through the use of inert matrices (IMs) to transmute plutonium and other minor actinides. These transuranic elements would then be embedded in an IM and placed in an appropriate reactor to facilitate transmutation [1].

Si₃N₄ has been identified as a candidate for use as an IM [2]. In order to determine whether a material is a viable candidate for use as an IM, its radiation tolerance must be tested. Among the main sources of radiation damage in a reactor core are fission fragments (FFs) [1,3]. Swift heavy ions (SHIs) have masses and energies that are very similar to those of FFs; they are an ideal means of simulating this form of irradiation. SHIs (in general masses > 100 amu and energies > 100 keV/amu) deposit energy, primarily through inelastic energy transfer mechanisms, to the electronic subsystem of the target material, which in some materials may lead to the formation of latent ion tracks. These latent tracks may be completely amorphous or consist of defective crystals; they may even be composed of a different phase than the unaffected material. In nuclear applications radiation effects limit the lifetime of reactor materials. Therefore, the modelling and prediction of microstructural modification resulting from ion irradiation provide considerable benefits [4].

The study of nanocrystalline materials is an important field of research. Nanocrystalline materials often behave differently in comparison with their larger grained counterparts, where grains are consistently larger than 100 nm. It has been shown that a decrease in grain size can result in changes in the general properties of materials—in particular, radiation stability [5–8], which is relevant to this investigation. On the one hand, a high density of grain boundaries can act as an efficient sink for the annihilation of interstitial defects and vacancies that are created during irradiation [5–9], which enhances radiation resistance. On the other hand, some forms of energy deposition promote the accumulation of radiation damage, due to the localized nature of energy deposition within an area much smaller than the grain diameter, i.e., on the nanometric scale [9–11]. The radiation damage mechanism in a nanostructured material is dependent on which of the above processes is dominant.

Silicon nitride is the only known nitride ceramic in which amorphous latent ion tracks have been observed. Its radiation behavior is therefore of interest. Most of the relevant literature has been concerned with the study of radiation-induced changes in the properties of amorphous thin-films [11–17] and polycrystals [12,18–22] of Si_3N_4 and closely related silicon nitride-based materials; data on the nano-crystalline state (*n*- Si_3N_4) are limited.

The microstructural effects of SHIs are most often studied using RBS, SAXS, AFM, FTIR, together with chemical etching [5,12–15,22–24]; however, transmission electron microscopy (TEM) is not often used [5,6,11,18–21]. TEM is the only direct method of analysis that can reveal the microstructural effects of SHIs. High resolution TEM enables the imaging of track characteristics, such as continuity/discontinuity and size (diameter), with minimal error.

The direct imaging of latent tracks and related defect structures serves as a tool for verifying different models that describe the interaction of SHIs with matter and, therefore, TEM techniques are well suited to the study of defects in individual crystallites, such as nanomaterials.

Therefore, the aim of this investigation is to analyze defects in *n*- Si_3N_4 that are related to swift heavy ion irradiation, using electron microscopy techniques to determine whether the observed microstructural changes in *n*- Si_3N_4 are different from those of polycrystalline Si_3N_4 .

2. Materials and Methods

Commercially available nanocrystalline powder Si_3N_4 (Sigma-Aldrich, 99.9% purity) placed on TEM grids were used as targets for irradiation. Specimens were irradiated with 714 and 670 MeV Bi, 156 MeV Xe to fluence $5 \times 10^{11} \text{ cm}^{-2}$ at U-400 and IC-100 cyclotrons in the FLNR of JINR (Dubna, Russia) and 220 MeV Xe to fluence $5 \times 10^{11} \text{ cm}^{-2}$ at DC-60 cyclotron in INP (Nur-Sultan, Kazakhstan). Aluminum foils of different thicknesses were used to alter the electronic stopping powers. Microstructural analysis was done with a JEOL JEM 2100 LaB6 or ARM200F TEM, both operated at 200 kV, at the Centre for HRTEM in Nelson Mandela University (Port Elizabeth, South Africa), and with a Talos™ F200i S/TEM operated at 200 kV at the FLNR, JINR (Dubna, Russia).

Experimental measurements for track diameters were done from dark field (DF) TEM images. In general, DF images contain less information related to strain, which yields a more accurate representation of true track diameter. To obtain a statistically significant average value for track diameters, between 50 and 100 tracks were measured. The total number of tracks measured from the DF TEM images were dependent on the number of tracks per sample, i.e., the ion fluence and the number of tracks that have the most reliable contrast for measurement purposes and the number of nanoparticles that could be located on the TEM grids.

Track diameter is measured through a line profile of the contrast across the track. Then, the track diameter (radius) is taken as the full width at half of the maximum FWHM of the intensity profile. There is always some uncertainty as to where the exact edge of the track is located—it does not have an abrupt onset, but rather a gradual slope, in terms of contrast decrease. Therefore, it is taken as the FWHM to provide some measure of the uncertainty in the location of the track edge. Each track is measured once across with some

integration in the width of the intensity profile. The uncertainty in the average track radius is the standard deviation, σ , of all measurements for a specific sample.

3. Results

A typical bright field (BF) TEM micrograph of nanocrystalline silicon nitride ($n\text{-Si}_3\text{N}_4$) irradiated with high-energy bismuth ions is shown in Figure 1. The tracks often appear slightly larger in this imaging mode because of strain contrast, which is not visible in dark field (DF) TEM.

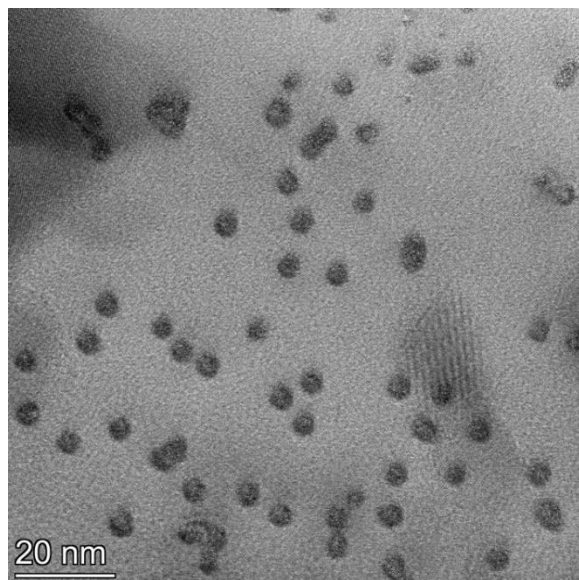


Figure 1. BF TEM image of $n\text{-Si}_3\text{N}_4$ irradiated with 670 MeV Bi ions.

The dependence of average track radius on electronic stopping powers, S_e , calculated with SRIM-2016, is shown in Figures 2 and 3. To modulate the stopping power, Al, degrader foils of varying thicknesses were used, except at the highest stopping power, where no foil was used. The degrader foil introduced a dispersion in the stopping power that increased with foil thickness. The dispersion for native stopping powers (no foil) was too small to be visible in Figure 2.

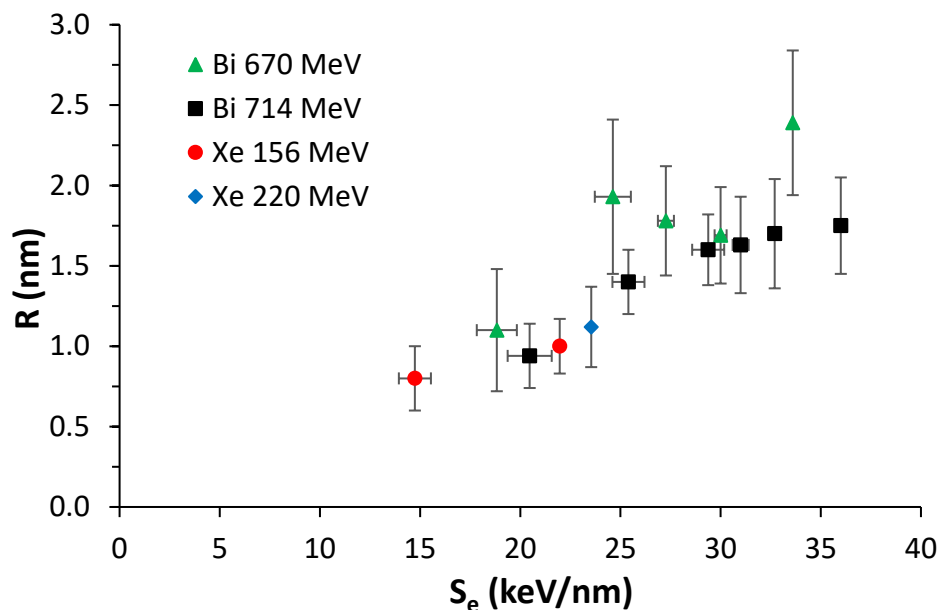


Figure 2. Electronic stopping powers (S_e) vs. average track radius in $n\text{-Si}_3\text{N}_4$.

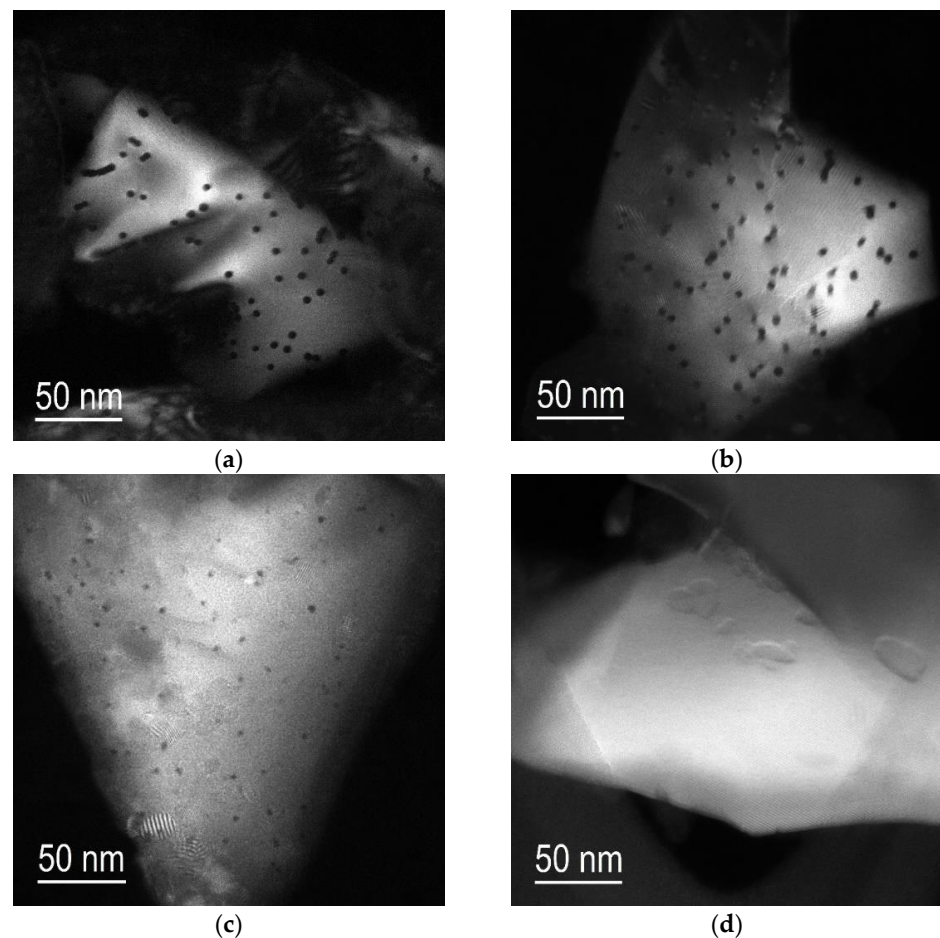


Figure 3. DF TEM images of $n\text{-Si}_3\text{N}_4$ irradiated with Bi ions at electronic stopping powers of (a) 36 keV/nm; (b) 29.4 keV/nm; (c) 20.5 keV/nm; and (d) 11.6 keV/nm.

The highest stopping power where no tracks were observed was 16.5 ± 1.2 keV/nm (714 MeV Bi with 27.7 μm Al degrader). At a stopping power of 14.5 ± 1.1 keV/nm (670 MeV Bi with 28.1 μm Al degrader), ion tracks were not continuous–amorphous, as was the case for all other observed ion tracks, but consisted of defect structures within the crystal. At a stopping power of 14.7 keV/nm (156 MeV Xe with 8 μm Al degrader), tracks were only observed in small nanoparticles (diameter < 30 nm) or on the edges of larger nanoparticles. Table 1 provides a summary of these stopping powers, where tracks were either not observed or in a different state, or observed only in special cases. Taking the average value of the highest stopping powers where tracks were observed as either defect structures or only on the edges of large particles and small particles or not observed (i.e., 14.7, 14.5, and 16.5 keV/nm as per the last three values in Table 1), we obtained an upper bound of 15.2 ± 1.0 keV/nm. Then, we took the lower bound as the lowest stopping power where tracks were not observed, i.e., 12.3 ± 0.8 keV/nm. This suggests that the threshold stopping power for track formation lies somewhere within the bounds of $12.3 \pm 0.8 < S_{et} < 15.2 \pm 1.0$ keV/nm.

Table 1. Summary of stopping powers where tracks are not formed, not amorphous, or only observed in special cases.

Ion/Energy (MeV)	Stopping Power (keV/nm)	State of Ion Tracks
$^{131}\text{Xe}/156$	12.3 ± 0.8	No Tracks
$^{131}\text{Xe}/156$	14.7 ± 0.8	Small particles and boundaries of large particles only
$^{209}\text{Bi}/670$	14.5 ± 1.1	Defect structures
$^{209}\text{Bi}/714$	16.5 ± 1.2	No Tracks

Track sizes were determined in polycrystalline (p-) Si_3N_4 irradiated under similar conditions (714 MeV Bi and 220 MeV Xe to fluence of $5 \times 10^{11} \text{ cm}^{-2}$). The measured radii in p- Si_3N_4 were $1.7 \pm 0.2 \text{ nm}$ and $1.0 \pm 0.2 \text{ nm}$ for bismuth and xenon ions, respectively [18–21]. Previous results and the data from this investigation for track radii showed similar values for poly- and nanocrystalline-silicon nitride, within the margin of error. This suggested that they have comparable radiation stabilities. The estimated threshold values for track formation in p- Si_3N_4 ($\sim 9 \text{ keV}$) [20,21] and n- Si_3N_4 ($12.3 \pm 0.8 < S_{et} < 15.2 \pm 1.0 \text{ keV/nm}$) in the present work differed appreciably, with the latter slightly lower than that in p- Si_3N_4 , with 3% Al contamination; however, it was quite similar to the estimated value from Zinkle et al. [19] of $\sim 15 \text{ keV/nm}$.

It should be noted that the polycrystalline samples of Si_3N_4 in [20,21] were found to contain low levels of aluminium contamination. The effect on the presence (and absence) of Al in p- Si_3N_4 is shown in [25], where one of the grains that had a marked lack of Al did not suffer amorphization or show evidence of latent ion tracks, as was observed in all other grains within the range of the implanted ions. The stopping power at the depth of the unaffected grain was $\sim 9 \text{ keV/nm}$. Accordingly, it is clear that the threshold for track formation was lowered in these samples, due to the presence of Al impurities. Available literature also supports the assertion that Si_3N_4 with very low impurity levels (99.5% to 99.9% purity), as used in this study, should have a higher threshold stopping power for track formation than impure Si_3N_4 [20,21,24]. However, the fact that grain size, especially nano-sized grains ($< 100 \text{ nm}$), play a role in the microstructural response of materials to SHIs should also be considered [5–11].

In Table 1, it is noted that at a stopping power of $14.7 \pm 0.8 \text{ keV/nm}$, tracks are only observed in small particles (size $< 30 \text{ nm}$) or close to the edges of larger particles. Molecular dynamics (MD) simulation of 700 MeV Bi ion track formation in nanocrystalline inclusions in a crystalline Si_3N_4 matrix [26] revealed that the track diameter inside the nanograin was systematically smaller, by approximately 15%, than the diameter in the surrounding material, where its size was close to the value calculated for single-crystal silicon nitride ($1.8 \pm 0.2 \text{ nm}$) [21]. This effect was observed for the inclusions with sizes $< 30 \text{ nm}$. This suggests that a grain size of 30 nm to 35 nm is close to the threshold of the heat confinement effect caused by grain boundaries. Therefore, it appears that this heat confinement effect may be responsible for the presence of ion tracks in small particles. The presence of ion tracks on the edges of some larger particles, as mentioned above, may be related to edge effects. Where the sample was at its thinnest, it could have been easier to form a latent ion track and/or to allow for the ejection of materials from the top and bottom surfaces of the particle, resulting in an area with lower density, similar to the process involved in hillock formation [27]. A track in a thinner area, compared to the interior of the particle, should be shorter; there, the average decrease in density, as viewed along the track, should appear to be more significant.

4. Conclusions

Based on experimentally measured track radii induced by 714 and 670 MeV Bi and 156 and 220 MeV Xe in n- Si_3N_4 , the threshold electronic stopping power was found to be within the following range: $12.3 \pm 0.8 < S_{et} < 15.2 \pm 1.0 \text{ keV/nm}$. The threshold stopping powers for pure p- and n- Si_3N_4 appeared to be quite similar, suggesting that they should

have similar radiation resistance. MD simulations and the results from this investigation suggested that the average grain size of n-Si₃N₄ in this study was above the threshold where the heat confinement effect may play a role in the evolution of ion track morphology and track radii, except in the case of a few isolated particles with very small grain size (<30 nm). The presence of ion tracks near the edges of larger particles in a sample, where they were otherwise lacking, was ascribed to decreased width at the edges, resulting in a more significant density (decrease)-to-length ratio. Therefore, the main conclusion based on the results of this study is that there is no clear difference in the microstructural evolution of p- and n-Si₃N₄.

Author Contributions: Conceptualization, A.J.v.V., A.I., V.S., A.A. and A.M.; methodology, A.J.v.V., A.M. and A.S.; validation, V.S., A.A., A.D. and M.Z.; formal analysis, A.J.v.V., A.I. and A.M.; investigation, A.J.v.V., A.I. and A.M.; resources, V.S., A.A., A.D. and M.Z.; data curation, A.J.v.V., A.I. and A.M.; writing—original draft preparation, A.J.v.V. and A.I.; writing—review and editing, V.S.; visualization, A.M. and A.S.; supervision, V.S., A.A. and A.D.; project administration, A.A. and V.S.; funding acquisition, A.A. and V.S. All authors have read and agreed to the published version of the manuscript.

Funding: This research was funded by the Ministry of Education and Science of the Republic of Kazakhstan (No. AP08856368, “Radiation resistance of ceramics based on nitrides and carbides in relation to the impact of heavy ions with energies of fission fragments”) and was supported by the Ministry of Science and Higher Education of the Russian Federation—contract 075-15-2021-709, unique identifier of the project RF-2296.61321X0037 (equipment maintenance).

Data Availability Statement: The data presented in this study are available on request from the corresponding author. The data are not publicly available due to funding requirements.

Acknowledgments: The authors thank the IC-100, U-400, and DC-60 accelerators staff of the Flerov Laboratory of Nuclear Research, Joint Institute for Nuclear Research, and Institute of Nuclear Physics.

Conflicts of Interest: The authors declare no conflict of interest.

References

1. Lee, Y.W.; Joung, C.Y.; Kim, S.H.; Lee, S.C. Inert matrix fuel—A new challenge for material technology in the nuclear fuel cycle. *Met. Mater. Int.* **2001**, *7*, 159–164. [[CrossRef](#)]
2. Yamane, J.; Imai, M.; Yano, T. Fabrication and basic characterization of silicon nitride ceramics as an inert matrix. *Prog. Nucl. Energy* **2008**, *50*, 621–624. [[CrossRef](#)]
3. Degueldre, C.; Paratte, J.M. Concepts for an inert matrix fuel, an overview. *J. Nucl. Mater.* **1999**, *274*, 1–6. [[CrossRef](#)]
4. Daraszewicz, S.L.; Duffy, D.M. Extending the inelastic thermal spike model for semiconductors and insulators. *Nucl. Instrum. Methods Phys. Res. B* **2011**, *269*, 1646–1649. [[CrossRef](#)]
5. Cureton, W.F.; Palomares, R.I.; Walters, J.; Tracy, C.L.; Chen, C.-H.; Ewing, R.C.; Baldinozzi, G.; Lian, J.; Trautmann, C.; Lang, M. Grain size effects on irradiated CeO₂, ThO₂, and UO₂. *Acta Mater.* **2018**, *160*, 47–56. [[CrossRef](#)]
6. Shen, T.D.; Feng, S.; Tang, M.; Valdez, J.A.; Wang, Y.; Sickafus, K.E. Enhanced radiation tolerance in nanocrystalline MgGa₂O₄. *Appl. Phys. Lett.* **2007**, *90*, 263115. [[CrossRef](#)]
7. Zhang, J.; Lian, J.; Fuentes, A.F.; Zhang, F.; Lang, M.; Lu, F.; Ewing, R.C. Enhanced radiation resistance of nanocrystalline pyrochlore Gd₂(Ti_{0.65}Zr_{0.35})₂O₇. *Appl. Phys. Lett.* **2009**, *94*, 243110. [[CrossRef](#)]
8. Nita, N.; Schaeublin, R.; Victoria, M. Impact of irradiation on the microstructure of nanocrystalline materials. *J. Nucl. Mater.* **2004**, *329–333*, 953–957. [[CrossRef](#)]
9. Liu, W.; Ji, Y.; Tan, P.; Zang, H.; He, C.; Yun, D.; Zhang, C.; Yang, Z. Irradiation Induced Microstructure Evolution in Nanostructured Materials: A Review. *Materials* **2016**, *9*, 105. [[CrossRef](#)]
10. Berthelot, A.; Hémon, S.; Gourbilleau, F.; Dufour, C.; Dooryhée, E.; Paumier, E. Nanometric size effects on irradiation of tin oxide powder. *Nucl. Instrum. Methods Phys. Res. Sect. B Beam Interact. Mater. At.* **1998**, *146*, 437–442. [[CrossRef](#)]
11. Grover, V.; Shukla, R.; Kumari, R.; Mandal, B.P.; Kulriya, P.K.; Srivastava, S.K.; Ghosh, S.; Tyagi, A.K.; Avasthi, D.K. Effect of grain size and microstructure on radiation stability of CeO₂: An extensive study. *Phys. Chem. Chem. Phys.* **2014**, *16*, 27065–27073. [[CrossRef](#)] [[PubMed](#)]
12. Kitayama, T.; Morita, Y.; Nakajima, K.; Narumi, K.; Saitoh, Y.; Matsuda, M.; Sataka, M.; Tsujimoto, M.; Isoda, S.; Toulemonde, M.; et al. Formation of ion tracks in amorphous silicon nitride films with MeV C60 ions. *Nucl. Instrum. Methods Phys. Res. Sect. B Beam Interact. Mater. At.* **2015**, *356*, 22–27. [[CrossRef](#)]
13. Komarov, F.F. Nano- and microstructuring of solids by swift heavy ions. *Phys. Usp.* **2017**, *60*, 435–471. [[CrossRef](#)]

14. Canut, B.; Ayari, A.; Kaja, K.; Deman, A.-L.; Lemiti, M.; Fave, A.; Souifi, A.; Ramos, S. Ion-induced tracks in amorphous Si_3N_4 films. *Nucl. Instrum. Methods Phys. Res. Sect. B Beam Interact. Mater. At.* **2008**, *266*, 2819–2823. [[CrossRef](#)]
15. Mota-Santiago, P.; Vazquez, H.; Bierschenk, T.; Kremer, F.; Nadzri, A.; Schauries, D.; Djurabekova, F.; Nordlund, K.; Trautmann, C.; Mudie, S.; et al. Nanoscale density variations induced by high energy heavy ions in amorphous silicon nitride and silicon dioxide. *Nanotechnology* **2018**, *29*, 144004. [[CrossRef](#)]
16. Vlasukova, L.A.; Komarov, F.F.; Yuvchenko, V.N.; Skuratov, V.A.; Didyk, A.Y.; Plyakin, D.V. Ion tracks in amorphous silicon nitride. *Bull. Russ. Acad. Sci. Phys.* **2010**, *74*, 206–208. [[CrossRef](#)]
17. Vlasukova, L.; Komarov, F.; Yuvchenko, V.; Baran, L.; Milchanin, O.; Dauletbekova, A.; Alzhanova, A.; Akilbekov, A. Etching of latent tracks in amorphous SiO_2 and Si_3N_4 : Simulation and experiment. *Vacuum* **2016**, *129*, 137–141. [[CrossRef](#)]
18. Morita, Y.; Nakajima, K.; Suzuki, M.; Narumi, K.; Saitoh, Y.; Ishikawa, N.; Hojou, K.; Tsujimoto, M.; Isoda, S.; Kimura, K. Surface effect on ion track formation in amorphous Si_3N_4 films. *Nucl. Instrum. Methods Phys. Res. Sect. B Beam Interact. Mater. At.* **2013**, *315*, 142–145. [[CrossRef](#)]
19. Zinkle, S.J.; Skuratov, V.A.; Hoelzer, D.T. On the conflicting roles of ionizing radiation in ceramics. *Nucl. Instrum. Methods Phys. Res. Sect. B Beam Interact. Mater. At.* **2002**, *191*, 758–766. [[CrossRef](#)]
20. Janse van Vuuren, A.; Ibrayeva, A.; Skuratov, V.; Zdorovets, M. Analysis of the microstructural evolution of silicon nitride irradiated with swift Xe ions. *Ceram. Int.* **2020**, *46*, 7155–7160. [[CrossRef](#)]
21. Janse Van Vuuren, A.; Ibrayeva, A.; Rymzhanov, R.A.; Zhalmagambetova, A.; O'Connell, J.H.; Skuratov, V.A.; Uglov, V.V.; Zlotski, S.V.; Volkov, A.E.; Zdorovets, M. Latent tracks of swift Bi ions in Si_3N_4 . *Mater. Res. Express* **2020**, *7*, 025512. [[CrossRef](#)]
22. Janse van Vuuren, A.; Ibrayeva, A.; Skuratov, V.A.; Zdorovets, M.V. iTS Model-Based Analysis of Track Formation in Crystalline and Amorphous Silicon Nitride. In Proceedings of the 13th International Conference of the Interaction of Radiation with Solids, Minsk, Belarus, 30 September–3 October 2019; pp. 97–99.
23. Sigrist, A.; Balzer, R. Untersuchungen zur Bildung von Tracks in Kristallen. *Helv. Phys. Acta* **1977**, *50*, 49–64. [[CrossRef](#)]
24. Komarov, F.F.; Vlasukova, L.A.; Kuchinskyi, P.V.; Didyk, A.Y.; Skuratov, V.A.; Voronova, N.A. Etched track morphology in SiO_2 irradiated with swift heavy ions. *Lith. J. Phys.* **2009**, *49*, 111–115. [[CrossRef](#)]
25. Janse van Vuuren, A.; Skuratov, V.; Ibrayeva, A.; Zdorovets, M. Microstructural Effects of Al Doping on Si_3N_4 Irradiated with Swift Heavy Ions. *Acta Phys. Pol. A* **2019**, *136*, 241–244. [[CrossRef](#)]
26. Rymzhanov, R.A.; Volkov, A.E.; Zhalmagambetova, A.; Zhumazhanova, A.; Skuratov, V.; Dauletbekova, A.K.; Akilbekov, A.T. Modelling of track formation in nanocrystalline inclusions in Si_3N_4 . *J. Appl. Phys.* **2022**, *132*, 085903. [[CrossRef](#)]
27. Ishikawa, N.; Taguchi, T.; Ogawa, H. Comprehensive Understanding of Hillocks and Ion Tracks in Ceramics Irradiated with Swift Heavy Ions. *Quantum Beam Sci.* **2020**, *4*, 43. [[CrossRef](#)]